Available online at www.sciencedirect.com
ScienceDirect
Polymer 48 (2007) 1388–1396
polymer
www.elsevier.com/locate/polymer

Novel triol-crosslinked polyurethanes and their thermorheological characterization as shape-memory materials

C.P. Buckley [a,*], C. Prisacariu [b], A. Caraculacu [b]

[a] Department of Engineering Science, University of Oxford, Parks Road, Oxford OX1 3PJ, UK
[b] Institute of Macromolecular Chemistry ''Petru Poni'', Aleea Grigore Ghica Voda, Nr. 41 A, Iasi 700487, Romania

Received 15 September 2006; received in revised form 19 December 2006; accepted 31 December 2006
Available online 5 January 2007

Abstract

A new family of crosslinked polyurethanes was synthesized and characterized as shape-memory polymers. Three-arm network junctions are provided by 1,1,1-trimethylol propane with an isocyanate group on each arm. Three diisocyanates are used: 4,4′-methylene bis(phenyl isocyanate), toluene diisocyanate, and 4,4′-dibenzyl diisocyanate. They are linked together by macrodiol soft segments formed from either polytetrahydrofuran with molar mass of 650, 1000 or 2000 g mol^{-1} or polycaprolactone glycol with molar mass of 830 or 1250 g mol^{-1}. Thermorheological response of each polymer was characterized by tensile creep tests through the glass transition of the soft segments, to obtain the linear viscoelastic retardation spectrum, limiting compliances and time–temperature shift factor. These were used to predict significant features of shape-memory performance. With a decrease in soft segment chain length, the temperature of maximum shape recovery rate increased and the width of the recovery window decreased, consistent with loss of soft segment chain mobility remote from the crosslinks. Tensile modulus in the switched condition (above T_g) was 8–16 MPa, increasing with crosslink density and hard-segment rigidity. The results confirmed the potential of these polyurethanes as a new family of tunable shape-memory materials.

Keywords: Polyurethane; Crosslinking; Shape-memory

1. Introduction

Polymers have great potential as shape-memory materials. The source of ''memory'' is their capacity to store preferred molecular orientation on large molecular length scales. The mechanism by which the shape memory is locked-in is usually cooling through the glass transition T_g (and consequent lengthening of mechanical relaxation times) or formation of a hard phase such as crystal domains. Shape recovery is triggered by subsequent heating, causing passage through T_g (and hence shortening of relaxation times) or softening of the hard phase. Lendlein and Kelch [1] provide a comprehensive review of the possibilities and of many of the shape-memory polymers proposed so far. It is clear that shape-memory behaviour is intrinsic to *any* polymer where molecular orientation arising from a prior stretch can be retained sufficiently at the orientation temperature. This will be the case where there exist chemical crosslinks, physical crosslinks provided by an entanglement network (with sufficiently long reptation time τ_d) or by a dispersed phase that is rigid to sufficiently high temperatures.

In practical applications of polymers as shape-memory materials, that is where they are acting as ''shape-memory polymers'' (SMP), a small set of parameters determine the usefulness, or otherwise, of a given polymer system for a given application. (1) The fractional recoverable strain: the maximum fraction of the imposed strain that can be recovered when triggered. (2) The temperature of maximum recovery rate T_{max} for a given rate of heating: a measure of the temperature required to trigger recovery of shape. (3) The width ΔT

* Corresponding author. Tel.: +44 1865 273156; fax: +44 1865 273906.
E-mail address: paul.buckley@eng.ox.ac.uk (C.P. Buckley).

0032-3861/$ - see front matter © 2007 Elsevier Ltd. All rights reserved.
doi:10.1016/j.polymer.2006.12.051

of the window of temperature within which shape recovery occurs. (4) The tensile modulus E_R at the temperature of full recovery: this determines the maximum shape-recovery restoring force if shape recovery is resisted. Since different applications make different demands on SMPs, it is particularly desirable to find polymer systems where parameters T_{max}, ΔT, and E_R are variable, so the same basic system can be tuned to suit different applications. Preferably, these will be systems where all the imposed strain is recoverable, that is the fractional recoverable strain is 100%.

Previous authors have highlighted the merits of polyurethane polymers as potential SMPs [1]. This arises largely from the chemical versatility of segmented polyurethane copolymer systems. Thus by suitable choice of diisocyanate and macrodiol phase-segregated materials may be produced, for example where one component comprises hard segments that provide physical crosslinking, to enable the retention of shape memory, while the other component provides a softer phase with a lower softening temperature, either glass transition or melting temperature, to enable the locking-in and release of shape memory at convenient temperatures. The softening temperature, which acts as the shape-memory trigger temperature (to be precise, T_{max}), may be changed systematically by variation of the hard-segment content [2–5] or the chain length of the macrodiol employed [6,7]. A feature of practical importance for biomedical applications of SMPs is the fact that these systems may be designed with trigger temperatures in the convenient range 20–50 °C [2,5–8].

The width of the trigger window ΔT is also important in applications of SMPs, but it has received little attention in previous published work. Nevertheless, published shape-recovery measurements, for example as reported by Lin and Chen [7] for polyurethanes, suggest values in the range 28–46 K, when T_{max} exceeds room temperature.

The third parameter, E_R, poses the greatest challenge for SMPs relative to shape-memory metal alloys, which are orders of magnitude stiffer. Shape recovery in polymers is usually driven by entropy-elastic recoil of molecular chains, but this is associated with extremely low elastic moduli, for example Young's moduli in the range 1–10 MPa. Thus there has been interest in reinforcing SMPs with hard particles such as chopped glass fibres [9], sub-micron SiC particles [10,11] or molecular-level mixing with silica [12]. However, the price for a small increase in E_R (e.g. to 10 MPa) may be a significant deterioration in the recoverability of shape, as observed by Ohki et al. [9]. Even 20% by weight of sub-micron SiC in a crosslinked epoxy gave only a 50% increase in shape restoring force [10].

The purpose of the present paper is to present a new family of potential polyurethane SMPs, addressing the issues discussed above. They are all produced by the prepolymer route using diisocyanate (DII) hard segments and macrodiol (MD) soft segments. Thus they have the usual versatility with respect to varying hard-segment content and macrodiol chain length, allowing the systematic variation of T_{max} and E_R (without using reinforcing particles). However, they are *also* single phase, chemically crosslinked polymers, and hence have the advantage of 100% recoverability of shape. This is achieved by employing a triol as chain extender, giving a network structure with tri-functional crosslinks. These polymers are characterized with respect to their thermorheological response in tension, in the linear viscoelastic regime. Then their performance in a shape-memory sequence is computed rigorously from the theory of temperature-dependent linear viscoelasticity, allowing comparisons to be made between them.

2. Experiments

2.1. Materials

Each member of the new family of SMPs was synthesized in our Iasi laboratory. The crosslinker triol used in all cases was 1,1,1-trimethylol propane (TMP). This was reacted with macrodiol and isocyanate in stoichiometric proportions to form a network polymer, with molar ratios TMP:MD:DII = 2:1:4. The MD was either polytetrahydrofuran (PTHF) or poly(caprolactone) diol (PCD), both with various chain lengths. The DII was chosen from the following three: the conventional diisocyanate with rigid structure, 4,4′-diphenyl diisocyanate (MDI); another common diisocyanate with a single phenyl group (TDI); and the third one was 4,4′-dibenzyl diisocyanate (DBDI). This last DII provides an interesting contrast with MDI, as it has more mobility because of rotation of the two benzene rings around the central $-CH_2-CH_2-$ bridge which links them [5]. This degree of freedom is not available to MDI, where the bridge is merely $-CH_2-$. A complete list of the polymers produced is given in Table 1. It includes a measure of crosslink density n_c for each material, expressed as the number of moles of three-arm stars per 100 g of polymer.

The synthesis route followed was of the prepolymer type, followed by melt casting of sheets. One mole of MD was dried under vacuum (1 mm Hg) at a temperature of 110 °C for 2 h. Then the vacuum was removed and after cooling to 90 °C, 4 mol of DII was added. After stirring for 30 s the prepolymer was obtained, with terminal NCO groups in a mixture with isocyanate excess. The last synthesis step was addition of

Table 1
List of the crosslinked polyurethane polymers sythesized and studied in this work

MD 1 mol	DII 4 mol	Moles of stars/100 g SMP
$PTHF_{650}$	2,4 + 2,6-TDI	0.1239
$PTHF_{650}$	MDI	0.1043
$PTHF_{650}$	DBDI	0.1013
$PTHF_{1000}$	DBDI	0.0861
$PTHF_{1000}$	MDI	0.0882
$PTHF_{1000}$	2,4 + 2,6-TDI	0.1018
$PTHF_{2000}$	DBDI	0.0602
$PTHF_{2000}$	MDI	0.0612
$PTHF_{2000}$	2,4 + 2,6-TDI	0.0505
PCD_{830}	DBDI	0.0928
PCD_{830}	MDI	0.0953
PCD_{830}	2,4 + 2,6-TDI	0.1115
PCD_{1250}	DBDI	0.0777

In every case, the crosslinker was trimethylol propane. For $PTHF_{2000}$ polymers, the glass transition was near to or below room temperature.

2 mol of the triol TMP as crosslinking agent, with vigorous stirring for 30 s. The ''pot life'' of this mix was about 5 min. Then the liquid mixture was cast into closed moulds lined with Teflon sheet and pre-heated to 90 °C so as to avoid interference from air humidity during the cure process. This process produced sheets approximately 1 mm thick. Post-cure was achieved by maintaining the moldings at 110 °C for 24 h. The polymers were demoulded after an additional 24 h at room temperature. No release agent was used.

The result is a network polymer with structure as shown schematically in Fig. 1. Each three-arm star is surrounded by three DII molecules, and these are linked together partly by the macrodiol. However, given the molar compositions of these polymers, there must also be some connectivity of junction points through just the DII, producing localities within the network with much reduced mobility – see dotted lines in Fig. 1.

In view of the constraint provided by the tri-functional crosslinks, these polymers are not expected to crystallize. To check this, wide-angle X-ray scattering (WAXS) patterns were obtained from two of the polymers with lowest crosslink density (and hence least constraint on crystallization) – DBDI/$PTHF_{2000}$ and MDI/$PTHF_{2000}$ – using copper Kα radiation. In both cases, the WAXS patterns showed only a single broad ''amorphous'' halo at $2\theta = 20°$, but no evidence for crystalline diffraction. From this it can be concluded that all the polymers in Table 1 are amorphous.

2.2. Thermorheological characterization

The thermorheological response of each polymer in Table 1 was characterized by a series of short-term tensile creep experiments in the linear viscoelastic region, in our Oxford laboratory. Rectangular bar specimens were machined from the moulded sheets with widths approximately 3 mm. Tests were carried out with a custom-made, lever-loading, creep apparatus with thermostatted heating chamber, using a 66 mm specimen length between the grips. In view of the high length/width ratio of each specimen and the fact that they were isotropic, tensile strain was determined from grip displacement, as end effects were negligible. The temperature was raised from ca 20 °C in a series of steps of duration of at least 15 min. At each step after temperature equilibration, the specimen was loaded with a creep stress in the linear viscoelastic range during a time of ca 0.5 s, and the axial strain $\varepsilon(t)$ was measured with an LVDT transducer and data logger, as a function of time t elapsed after loading. The duration of constant stress was 30 s, and then the stress was removed for at least 300 s to allow close to full recovery of strain before the next temperature step. The tensile creep compliance was determined from the strain during the creep period, and the applied tensile stress σ thus: $D(t) = \varepsilon(t)/\sigma$. A typical set of creep curves is shown for material DBDI/PCD_{1250} in Fig. 2.

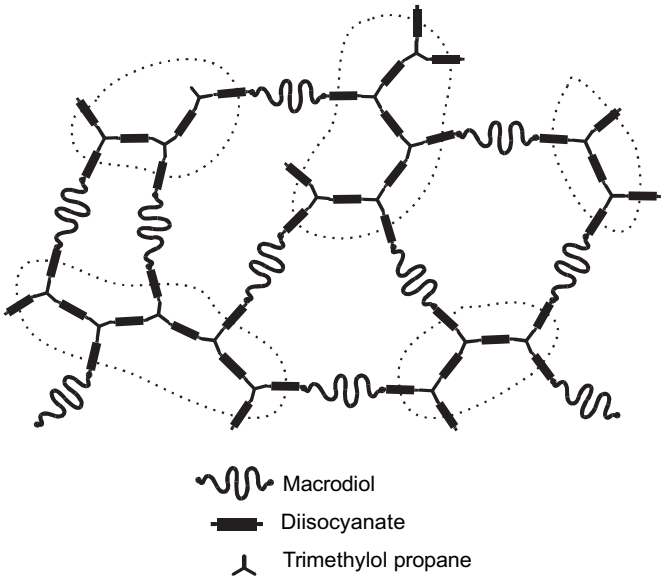

Fig. 1. Schematic diagram of the structure of the triol-crosslinked polyurethanes. Dashed lines indicate DII-rich regions of reduced mobility.

3. Theory of shape memory for a linear viscoelastic solid

3.1. General relations

Several authors have proposed dedicated, empirical, constitutive models for capturing shape-memory response in polymers [13–15]. In the context of small strain linear viscoelasticity this is unnecessary. The shape-memory effect is calculable rigorously from standard theory. Here, however, we re-cast the standard theory slightly, for convenience in describing shape-memory behaviour. For the present purpose an one-dimensional description is sufficient.

Consider the case of a linear viscoelastic polymer in its glass transition region. At reference temperature T^* it has normalized retardation spectrum $\varphi^*(\ln\tau)$, unrelaxed compliance D^*_U and relaxed compliance D^*_R, where $D^*_R \gg D^*_U$. In the present context, an important consideration is the effect of temperature on viscoelastic response. In the analysis that follows we make two important assumptions concerning this. First, consistent with many previous observations of polymers at the glass transition, we take the retardation times to scale uniformly when

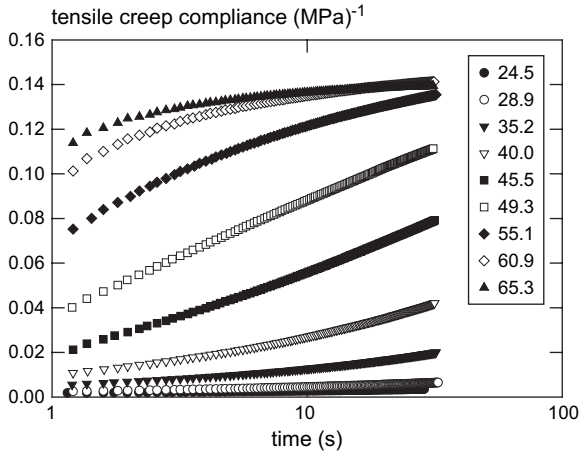

Fig. 2. A typical set of tensile creep curves for various temperatures (°C), in this case for polymer DBDI/PCD_{1250}.

temperature is changed, through the temperature-dependent scaling factor a_T. Thus, at an arbitrary temperature we have

$$\varphi(\ln\tau) = \varphi^*(\ln(a_T\tau)). \tag{1}$$

Second, we note that the relaxed compliance corresponds to the rubber elastic compliance, that is $D_R = E_R^{-1}$. Moreover from the molecular theories of entropic rubber elasticity, at temperature T we expect [16] $E_R \propto \rho T$ where ρ is the density at temperature T. However, at temperatures of interest in the present work, temperature dependence of E_R was dominated by T rather than ρ (the latter contributing only ca 20%). Hence at an arbitrary temperature T we have, to a good approximation

$$D_R = (T^*/T)D_R^*; \quad \Delta D \equiv D_R - D_U \cong (T^*/T)\Delta D^*. \tag{2}$$

As is customary, viscoelastic response in the linear region may be represented as the response of a generalized Voigt model, with normalized distribution of retardation times $\varphi(\ln\tau)$. Thus, at any arbitrary time t, when the temperature is T and the stress acting is σ, the total strain response may be written as the weighted sum of a spectrum of internal viscoelastic strains $\varepsilon^v(t,\ln\tau)$ and an elastic strain $\varepsilon^e(t) = D_U\,\sigma(t)$ thus

$$\varepsilon(t) = \int_{-\infty}^{\infty} \varphi(\ln\tau)\varepsilon^v(t,\ln\tau)\ \mathrm{d}\ln\tau + D_U\sigma(t). \tag{3}$$

Also, evolution of the viscoelastic strain spectrum is given by the equation of a single Voigt model, with retardation time τ and relaxed compliance ΔD:

$$\tau\frac{\partial\varepsilon^v}{\partial t} + \varepsilon^v = \Delta D\,\sigma. \tag{4}$$

Expressed as the spectrum of internal strains at the reference temperature ε^{v*}, the general solution of Eq. (4) for a stress history $\sigma(u)$ is as follows:

$$\varepsilon^{v*}(t,\ln\tau) = \int_{-\infty}^{t} \frac{T^*}{T(u)}\frac{\Delta D^*}{a_T(u)\tau}\exp\left[-\left(\frac{t}{a_T(t)\tau} - \frac{u}{a_T(u)\tau}\right)\right] \times \sigma(u)\,\mathrm{d}u. \tag{5}$$

This function expresses completely the memory of the prior stress/temperature history at time t.

Since the present paper concerns shape recovery, the prediction of strain during recovery under zero stress is of special interest. Take the starting time of the unloaded period to be t_u, such that

$$\sigma(u) = 0 \quad \text{for all } u > t_u. \tag{6}$$

Then the solution to Eq. (4) becomes (for $t > t_u$)

$$\varepsilon^{v*}(t,\ln\tau) = \varepsilon^{v*}(t_u,\ln\tau)\exp\left(-\frac{\Delta\xi}{\tau}\right). \tag{7}$$

where $\Delta\xi$ is a reduced recovery time given by

$$\Delta\xi = \int_{t_u}^{t} \frac{\mathrm{d}u}{a_T(u)}. \tag{8}$$

Combining Eqs. (3) and (7), we obtain the total strain remaining at time t during the recovery period $t > t_u$:

$$\varepsilon(t) = \int_{-\infty}^{\infty} \varphi^*(\ln\tau)\varepsilon^{v*}(t_u,\ln\tau)\exp\left(-\frac{\Delta\xi}{\tau}\right)\mathrm{d}\ln\tau. \tag{9}$$

3.2. Application to thermorheological characterization

We first apply the above equations to thermorheological characterization of the present materials. Consider the case of isothermal creep experiments under a constant stress, as used in this work to characterize each material. Eqs. (2), (3) and (5) give the creep compliance at time t after loading, at temperature T:

$$D(t) = \frac{T^*}{T}\left(D_R^* - \Delta D^*\int_{-\infty}^{\infty}\varphi^*\exp\left(-\frac{\xi}{\tau}\right)\mathrm{d}\ln\tau\right). \tag{10}$$

where $\xi = t/a_T$ is the reduced creep time. Thus it is clear that a creep master curve for the reference temperature may be constructed by combining creep curves for various temperatures:

$$D^*(t) = \left(\frac{T}{T^*}\right)D(a_T t). \tag{11}$$

First the creep compliance function for each temperature is multiplied by the factor T/T^*, and then time–temperature superposition is applied on a logarithmic time scale. Repeating this process with a number of creep curves allows a composite "master" creep curve to be build up for the reference temperature, spanning a much wider range of time than was available experimentally.

This approach has been applied with success many times in the past, especially to amorphous polymers in the glass transition region [16]. It was applied here to all the materials in Table 1 except the three based on $PTHF_{2000}$, for which the glass transition was found to be close to or below room temperature and insufficient creep data were available. Between nine and twelve individual isothermal creep curves were used to create each master creep curve. The time–temperature shift factor function a_T was found empirically, from the horizontal shift $\ln a_T$ required to superpose the graphs of $(T/T^*)D$ on a logarithmic time scale. For present purposes $\ln a_T$ was fitted to a quadratic function of temperature for each polymer.

For comparing the relaxation processes for various polymers, it was helpful to compute the retardation spectrum for each. The procedure adopted was first to fit each master curve to an empirical creep function: a new skewed form of the widely used Kohlrausch–Williams–Watts (KWW) stretched exponential function:

$$D^* = D_R^* - \Delta D^* \exp\left\{ -\left(\frac{t}{\tau_0}\right)^{[\beta - \gamma \ln(t/\tau_0)]} \right\}. \quad (12)$$

Here $\beta < 1$ gives broadening of the relaxation relative to the single retardation time case, and $\gamma > 0$ corresponds to a skewing of the relaxation, with stretching of the spectrum at long time scales and narrowing at short time scales. Clearly, Eq. (12) is meaningful only within the range $\ln(t/\tau_0) < \beta/\gamma$, however, this value of $\ln(t/\tau_0)$ lies far beyond the times of interest. The case $\gamma = 0$ corresponds to the usual KWW function. In the present work it was found that creep curves (plotted on a logarithmic time axis) sometimes showed significant deviation from the KWW function, and the skewed form of Eq. (12) gave a significantly closer fit, with values of the parameter γ lying in the range -0.0042 to $+0.008$, and with values of β spanning the range 0.27–0.44. A typical master curve and its corresponding fitted function is shown for material DBDI/PTHF$_{650}$ in Fig. 3, showing the quality of fit obtained (ignoring the first few data points of each creep curve because of perturbation arising from the finite time taken to apply the creep load).

Finally, the retardation spectrum $\varphi^*(\ln \tau)$ was computed from the function in Eq. (12), employing a third order Schwarzl–Staverman approximation [17], and using analytical differentiation to obtain the three derivatives required

$$\frac{dD^*}{d(\ln t)}, \frac{d^2D^*}{d(\ln t)^2}, \frac{d^3D^*}{d(\ln t)^3}.$$

Some of the resulting normalized retardation spectra are compared in Fig. 4, reduced to a temperature of $T = 92.3\ ^\circ C$, which is the mean of the reference temperatures used in constructing the creep master curves.

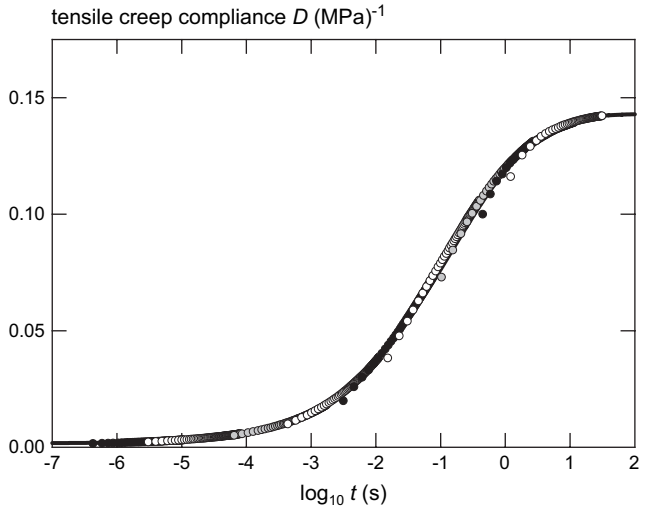

Fig. 3. The creep master curve for polymer DBDI/PCD$_{1250}$ for a reference temperature $T^* = 65.3\ ^\circ C$, obtained by horizontal shifting of $(T/T^*)D(\ln t)$ for the curves in Fig. 2.

3.3. Prediction of shape-memory performance

In this paper we compare the materials in Table 1 with respect to their predicted performance in the idealized shape-memory sequence illustrated schematically in Fig. 5. It comprises four steps. (a) The material is subjected to a constant stress σ_0 at a constant temperature T_{high} that lies well above the glass transition temperature T_g. This causes creep to a maximum strain ε_m. (b) The temperature is lowered instantaneously to a temperature T_{low} that is well below T_g. According to Eq. (5) this leads in general to additional, thermally induced, creep as noted by McCrum [18]. However, we choose T_{low} to be so far below T_g that retardation times are all sufficiently lengthened that negligible additional creep occurs. (c) The material is unloaded at time t_u. The strain just before unloading is the maximum strain reached ε_m, while the strain just after unloading is ε_u. The latter strain is 'locked-in' because of the length of the retardation times at temperature T_{low}, until recovery occurs. The strain recovered instantaneously on unloading is

$$\varepsilon_m - \varepsilon_u = D_U(T_{low})\,\sigma_0. \quad (13)$$

(d) Temperature is now raised at a constant rate $\dot{T}$, causing recovery to occur, with maximum recovery rate at temperature T_{max} and a recovery window of width ΔT, see Fig. 5.

From Eq. (5) it follows that, under the conditions described above, the distribution of internal strains is uniform at $t = t_u$, with value

$$\varepsilon^{v*}(t_u, \ln \tau) = \left(\frac{T^*}{T_{high}}\right)\Delta D^* \sigma_0 \quad \text{for all } \tau. \quad (14)$$

Moreover, since the spectrum φ in Eq. (3) is normalized, and after unloading we have $\sigma = 0$ it follows from Eq. (3) that the overall strain ε_u also has the value given by Eq. (14). Hence, invoking Eq. (9), we see that the fractional recovery at time $t > t_u$, for this particular prior history, is given by

$$f(t) \equiv \frac{\varepsilon_u - \varepsilon(t)}{\varepsilon_u} = 1 - \int_{-\infty}^{\infty} \varphi^* \exp\left(-\frac{\Delta\xi}{\tau}\right) d\ln\tau. \quad (15)$$

For each of the materials in Table 1 not based on PTHF$_{2000}$, this function was computed for a heating rate of 0.1 K s^{-1}. The plot in Fig. 6 is a typical result.

4. Results and discussion

4.1. Shape-recovery temperature

Figs. 7 and 8 summarise the calculated values of T_{max} and ΔT, respectively. They show two dominant features. Firstly, for given chemical composition, T_{max} increases while ΔT decreases as the density of crosslinks increases, as expressed by n_c. Secondly, there are significant differences between polymers with different DII components. It is notable that the TDI-based polymers have lower T_{max} and higher ΔT than polymers based on MDI or DBDI.

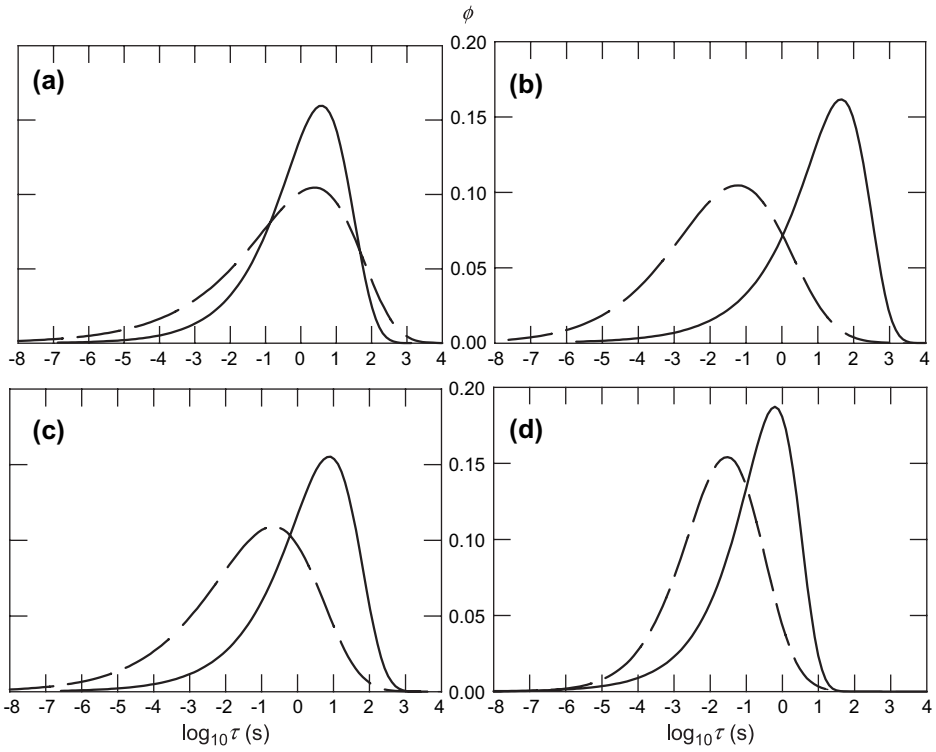

Fig. 4. A selection of normalized retardation spectra, obtained from creep master curves, for pairs of polymers with the same chemical composition but differing macrodiol chain length. They all refer to a temperature of 92.3 °C (the mean reference temperature). In each case the full line refers to the shorter chain MD and the dashed line to the longer chain MD. (a) TDI/$PTHF_{650}$ and TDI/$PTHF_{1000}$; (b) MDI/$PTHF_{650}$ and MDI/$PTHF_{1000}$; (c) DBDI/$PTHF_{650}$ and DBDI/$PTHF_{1000}$; (d) DBDI/PCD_{830} and DBDI/PCD_{1250}.

The effect of varying crosslink density may be explained in terms of the network structure shown schematically in Fig. 1. For polymers comprising the same chemical components – that is, for points with the same symbols in Figs. 7 and 8 – variation in crosslink density arises solely from change in length of the soft segment MD chains. When they are end linked to the extended network junctions, through relatively less mobile DII segments, their mobility is highly restricted, lengthening their retardation times. Portions of the MD chains more remote from the junctions are more mobile, with shorter retardation times. According to this picture, when n_c increases it is because of a shortening of MD chains; hence there is a reduced contribution to the retardation spectrum from the shortest retardation

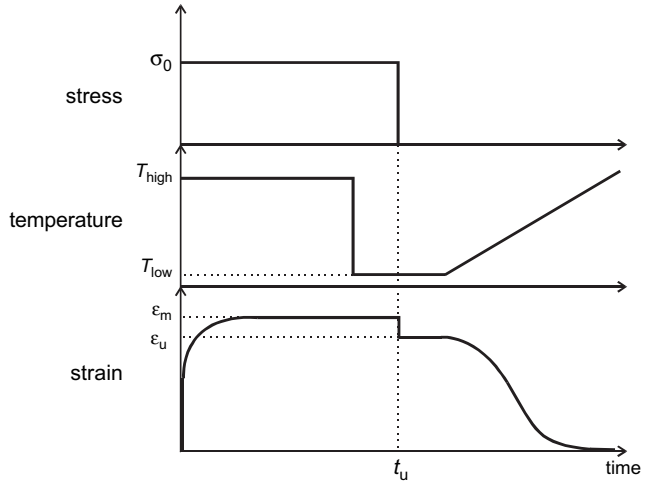

Fig. 5. Schematic diagram of the shape-memory sequence modelled using linear viscoelasticity, in order to compare the shape-memory performance of the polymers.

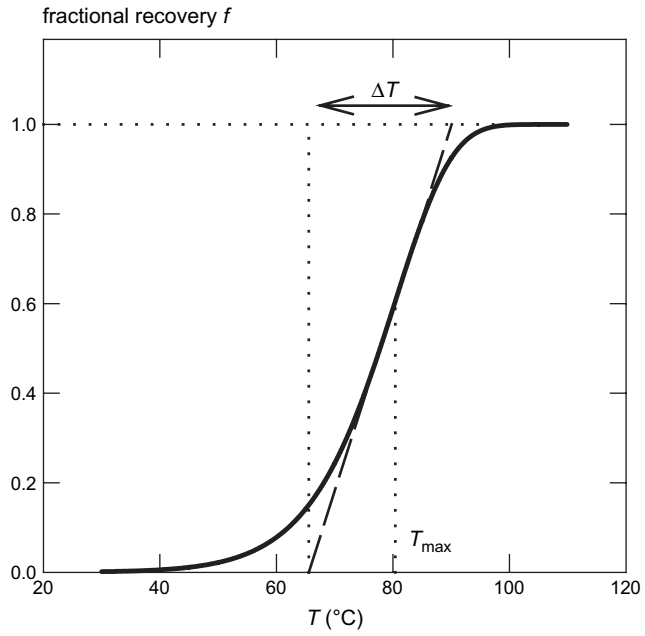

Fig. 6. Graph showing the calculated fractional recovery of polymer DBDI/$PTHF_{650}$, for heating at 0.1 $K\,s^{-1}$, indicating the temperature T_{max} of maximum recovery rate and the width ΔT of the recovery window.

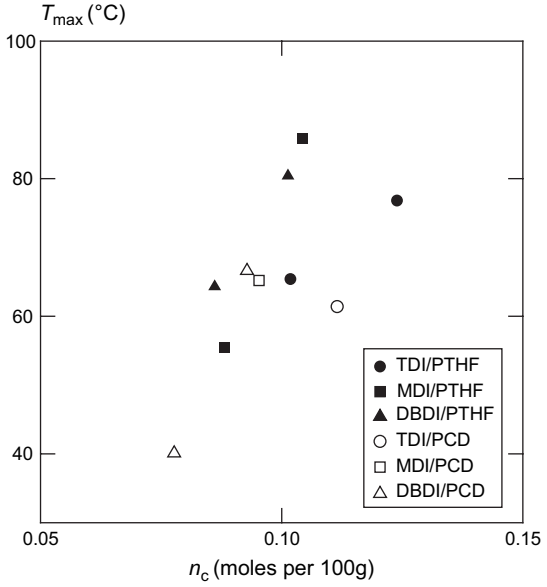

Fig. 7. Calculated temperature of maximum recovery rate T_{max} during simulated shape recovery for a heating rate of 0.1 K s^{-1}, plotted versus crosslink density, expressed as the number of moles of 3-arm star crosslinks per 100 g: n_c.

times, while the longer retardation times are relatively unaffected. In addition there is an increase in volume fraction of the DII-rich regions of reduced mobility indicated in Fig. 1. It follows that there is expected to be a narrowing of the soft segment retardation spectrum and an overall shift to longer times.

This is precisely the effect seen in the four plots in Fig. 4. The lines in each plot refer to pairs of polymers with the same chemical components but differing MD chain length. The full line refers to a shorter chain length than that for the dashed line, and in each case it may be seen that there is a narrowing of the spectrum and shift of its peak to longer times (although the shift is small in the case of Fig. 4(a)). From linear viscoelasticity theory as outlined above, this would be predicted to lead to an increase in shape-memory trigger temperature T_{max} and decrease in width ΔT of the shape-recovery temperature window, as observed in the present predictions of shape-memory response. Strictly, this conclusion requires that the temperature sensitivity of ln a_T is similar for all the polymers, but this was the case to a sufficient approximation (d ln a_T/dT at the reference temperature varied between -0.12 K^{-1} and -0.29 K^{-1}).

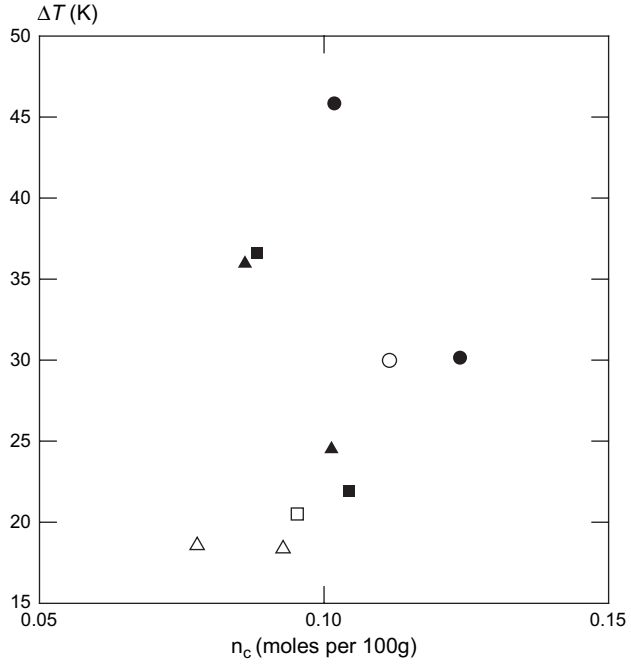

Fig. 8. Calculated width ΔT of the recovery window, during simulated shape recovery for a heating rate of 0.1 K s^{-1}, plotted versus crosslink density. Symbols are as indicated in Fig. 7.

The effects of varying hard segment in Figs. 7 and 8 may be attributed to the differing mobility of TDI as compared to MDI and DBDI. Each molecule of TDI is smaller, containing only one phenyl ring, compared to MDI and DBDI which have two phenyl rings. This is expected to lead to greater soft segment mobility for TDI-based polymers, and hence to a lower T_{max}, as seen, for equal crosslink density. However, the commercially produced TDI used in the present work is a blend of two isomers: 2,4-TDI (80%) and 2,6-TDI (20%), which would be expected to have different mobilities. Thus a broader retardation spectrum and wider shape-recovery window would be expected compared to MDI and DBDI, as seen in Fig. 8. It is also interesting to note that the PCD-based polymers show narrower recovery windows than those based on PTHF, reflecting their narrower spectra (see Fig. 4).

4.2. Relaxed modulus

Also of great interest in relation to shape-memory performance is the relaxed modulus E_R. This determines the recovery stress available, in the event that shape recovery during heating is resisted. It is simply the reciprocal of D_R. Fig. 9 shows results plotted versus crosslink density, compared with the classical predictions from the competing affine and phantom chain theories of rubber elasticity, respectively [19]:

$$E_R(\text{affine}) = 3\mu k_B T/2 \quad E_R(\text{phantom}) = \mu k_B T/2. \tag{16}$$

where $\mu = 10\rho N_A n_c$ is the number density of tri-functional network junction points, N_A is Avogadro's number and ρ is the density (here approximated as 1150 kg m^{-3} for all the materials). It is clear that there is good agreement with the theory, to within the uncertainty in the theory; all the data points lying essentially between the two predictions. However, there is also significant influence of chemical composition. In particular it is interesting to note the order of stiffness for polymers based on the three DIIs: MDI > DBDI > TDI. This also reflects the relative intrinsic stiffness of the DII groups. In particular, it is significant that MDI (relatively rigid DII) gave polymers with E_R in good agreement with the affine deformation theory, where junction points are assumed to be immobile and to move affinely with the deformation. Conversely, the more flexible DIIs DBDI and TDI gave polymers with E_R closer to the phantom chain (mobile junction point) theory. An important

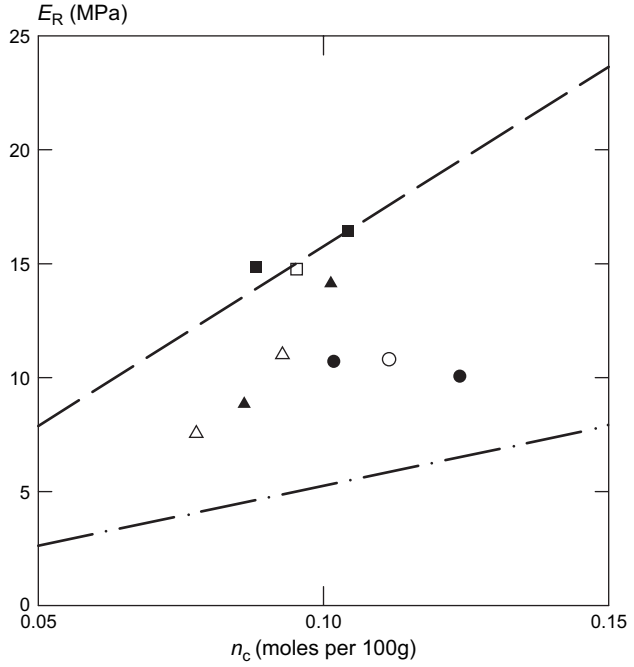

Fig. 9. Tensile modulus in the relaxed (rubbery) state, plotted versus crosslink density for a temperature of 92.3 °C. The dashed line is the prediction of the affine network theory of rubber elasticity, while the dash-dotted line is the prediction of the phantom chain theory of rubber elasticity. Symbols are as indicated in Fig. 7.

practical point for shape-memory applications is that the values of E_R found in this work (8–16 MPa) are relatively high for an unreinforced polymer in the rubbery state: a desirable feature for a shape memory polymer, giving rise to a relatively high restoring force if recovery is resisted.

5. Conclusions

The new triol-crosslinked polyurethanes appear to have great potential as shape-memory polymers. Complete recovery is ensured by chemical crosslinking through a triol, while adjustment of the shape-memory trigger temperature is achieved by variation of the chemical composition of the hard and soft segments, and the chain length of the soft segments. Three hard segments were examined (MDI, TDI and DBDI), together with two soft segments (PTHF and PCD) with molar masses from 650 to 2000. By appropriate choice of these, the trigger temperature has been varied from below room temperature up to 86 °C, illustrating the versatility of the system. The shape-memory performance of these materials was predicted rigorously, by first measuring their thermorheological response in the linear viscoelastic region, and then predicting their shape recovery during the heating phase in a standard shape-memory test.

The predicted temperature of peak recovery rate T_{max} increased with crosslink density for any given combination of DII and MD, as a result of decreased molecular mobility, revealed through shifting of the retardation spectra to longer times. The greater flexibility of TDI was also apparent, as compared to MDI and DBDI, producing a lower T_{max} for given crosslink density. The width of the shape-recovery temperature window ΔT was found to decrease with decreasing MD chain length. The retardation spectra revealed that this was caused primarily by a suppression of the shortest retardation times. The shorter chain length reduced the mobility of the portions of MD chains most remote from the influence of the hard segments at the network junctions. In addition there was a clear influence of the presence of the two isomers in TDI, causing a large increase (approximately a doubling) of ΔT relative to polymers based on MDI or DBDI.

The rubbery-state modulus E_R showed a trend of increasing with crosslink density, with measured values lying close to or between the predictions of the affine and phantom chain theories of rubber elasticity. However, there was also an influence from the chemical composition, with the actual values between these two limits reflecting the intrinsic stiffnesses of the three DIIs and hence the molecular mobility at the network junctions. These results illustrate the potential of this family of PUs to act as shape-memory polymers, and to be tailored chemically to suit particular practical applications.

Acknowledgements

The authors are grateful for financial support from the Royal Society of London in the form of a Joint Project Grant, and from NATO in the form of a Collaborative Linkage Grant. They also acknowledge valuable technical assistance provided by Mr Victor Prisacariu.

References

[1] Lendlein A, Kelch S. Shape-memory polymers. Angewandte Chemie International Edition 2002;41:2035–57.
[2] Lin JR, Chen LW. Study on shape-memory behavior of polyether-based polyurethanes. I. Influence of the hard-segment content. Journal of Applied Polymer Science 1998;69:1563–74.
[3] Lee BS, Chun BC, Chung Y-C, Sul KI, Cho JW. Structure and thermomechanical properties of polyurethane block copolymers with shape memory effect. Macromolecules 2001;34:6431–7.
[4] Yang JH, Chun BC, Chung Y-C, Cho JH. Comparison of thermal/mechanical properties and shape memory effect of polyurethane block-copolymers with planar or bent shape of hard segment. Polymer 2003;44:3251–8.
[5] Wang W, Ping P, Chen X, Jing X. Polylactide-based polyurethane and its shape-memory behavior. European Polymer Journal 2006;42:1240–9.
[6] Takahashi T, Hayashi N, Hayashi S. Structure and properties of shape-memory polyurethane block copolymers. Journal of Applied Polymer Science 1996;60:1061–9.
[7] Lin JR, Chen LW. Study on shape-memory behavior of polyether-based polyurethanes. II. Influence of soft-segment molecular weight. Journal of Applied Polymer Science 1998;69:1575–86.
[8] Kim BK, Lee SY, Xu M. Polyurethanes having shape memory effects. Polymer 1996;37:5781–93.
[9] Ohki T, Ni Q-Q, Ohsako N, Iwamoto M. Mechanical and shape memory behaviour of composites with shape memory polymer. Composites Part A 2004;35:1065–73.
[10] Gall K, Dunn ML, Liu Y, Finch D, Lake M, Munshi NA. Shape memory polymer nanocomposites. Acta Materialia 2002;50:5115–26.

[11] Liu Y, Gall K, Dunn ML, McCluskey P. Thermomechanics of shape memory polymer nanocomposites. Mechanics of Materials 2004;36: 929–40.
[12] Cho JW, Lee SH. Influence of silica on shape memory effect and mechanical properties of polyurethane–silica hybrids. European Polymer Journal 2004;40:1343–8.
[13] Tobushi H, Okumura K, Hayashi S, Ito N. Thermomechanical constitutive model of shape memory polymer. Mechanics of Materials 2001;33:545–54.
[14] Liu Y, Gall K, Dunn ML, Greenberg AR, Diani J. Thermomechanics of shape memory polymers: Uniaxial experiments and constitutive modelling. International Journal of Plasticity 2006;22:279–313.
[15] Diani J, Liu Y, Gall K. Finite strain 3D thermoviscoelastic constitutive model for shape memory polymers. Polymer Engineering and Science 2006;46:486–92.
[16] Ferry JD. Viscoelastic properties of polymers. 3rd ed. New York: John Wiley and Sons; 1980.
[17] Tschoegl NW. The phenomenological theory of linear viscoelastic behavior. Berlin: Springer-Verlag; 1989.
[18] McCrum NG. The determination of $\mathrm{d}\ln r^2/\mathrm{d}T$ by the method of temperature induced creep in tension and torsion. Polymer 1986;27:47–60.
[19] Erman B, Mark JE. Structures and properties of rubber-like networks. New York: OUP; 1997.